Net exchange reformulation of radiative transfer in the CO_2 15μm band on Mars.

Jean-Louis Dufresne [1*], Richard Fournier[2]
Christophe Hourdin [1†], Frédéric Hourdin[1]

[1] *Laboratoire de Météorogogie Dynamique, IPSL;*
CNRS and Université Pierre et Marie Curie; Paris; France
[2] *Laboratoire d'Energétique;*
Université Paul Sabatier; Toulouse; France

To be pulished in *J. Atm. Sci.*

Abstract

The Net Exchange Formulation (NEF) is an alternative to the usual radiative transfer formulation. It was proposed by two authors in 1967, but until now, this formulation has been used only in a very few cases for atmospheric studies. The aim of this paper is to present the NEF and its main advantages, and to illustrate them in the case of planet Mars.

In the NEF, the radiative fluxes are no more considered. The basic variables are the net exchange rates between each pair of atmospheric layers i, j. NEF offers a meaningful matrix representation of radiative exchanges, allows to quantify the dominant contributions to the local heating rates and provides a general framework to develop approximations satisfying reciprocity of radiative transfer as well as first and second principle of thermodynamic. This may be very useful to develop fast radiative codes for GCMs.

We present a radiative code developed along those lines for a GCM of Mars. We show that computing the most important optical exchange factors at each time step and the others exchange factors only a few times a day strongly reduces the CPU time without any significant precision lost. With this solution, the CPU time increases proportionally to the number N of the vertical layers and no more proportionally to its square N^2. We also investigate some specific points such as numerical instabilities that may appear in the high atmosphere and errors that may be introduced if inappropriate treatments are performed when reflection at the surface occurs.

*Corresponding author: Laboratoire de Météorologie Dynamique, Université P. et M. Curie - Boite 99, F-75252 Paris Cedex 05 - France. E-mail: dufresne@lmd.jussieu.fr

†Now at Laboratoire d'Océanographie Physique, Museum National d'Histoire Naturelle, Paris

1 Introduction

In the past decades, numerical modeling of the atmospheric circulation of Mars has been taking an increasing importance, in particular in the frame of the spatial exploration of the red planet (Leovy and Mintz, 1969; Pollack et al., 1981; Hourdin et al., 1993; Forget et al., 1998). With the increased number of missions to Mars and especially with the use of aero-assistance for orbit injection, there is an increasing demand for improvements of our knowledge of Martian physics, in particular of Martian upper atmosphere.

Computation of radiative transfer is a key element in the modeling of atmospheric circulation. Absorption and emission of visible and infrared radiation are the original forcing of atmospheric circulation. With typical horizontal grids of a few thousands to 10.000 points, and since we want to cover years with explicit representation of diurnal cycle, operational radiative codes must be extremely fast. Representation of radiative transfer must therefore be drastically simplified and parameterized.

For Mars, the main contributors to atmo-

spheric radiation are by far carbon dioxide (which represents about 95% of the atmospheric mass) and airborne dust particles (even outside large planetary scale dust-storms, extinction of solar light by dust is of several tens of percent). Carbon dioxide is dominant at infrared frequencies with a vibration-rotation line spectrum that must be properly accounted for.

In the development phase of the Laboratoire de Météorologie Dynamique (LMD) Martian atmospheric circulation model, a major step was the derivation of a radiative transfer code for the CO_2 15 μm band (Hourdin, 1992). This model was based upon the Wide Band Model approach developed by Morcrette et al. (1986), and used in the operational model of the European Center for Medium-Range Weather Forecasts (Morcrette, 1990). This model is based on a two stream flux formulation. Wide band transmitivities are fitted as Padé approximants (ratio of two polynomials) as functions of integrated absorber amounts, including simple representations of temperature and pressure dependencies. For application to Martian atmosphere, the fit was somewhat adapted in order to account for Doppler line broadening which becomes significant above 50 km.

Altogether, in standard configurations of the LMD Martian model with a 25 layer vertical discretization, infrared computations represent a significant part (up to one half) of the total computational cost. Similar reports are made concerning terrestrial models. The transmission functions being not multiplicative for band models, the determination of radiative fluxes at each level requires independent calculations of the contributions of all atmospheric layers. The corresponding computation cost increases as the square of the number of vertical layers. This quadratic dependency undoubtedly represents a severe limitation when thinking of further model refinements, in particular as far as near surface and high atmosphere processes are concerned, both requiring significant vertical discretization increases. However, it is commonly recognized that, despite of this formal difficulty, infrared radiative transfers are dominated by a few terms such as cooling to space and short distance exchanges (e.g. Rodgers and Walshaw, 1966; Fels and Schwarzkopf, 1975). In practice, the quadratic dependency of absorbtivity-emissivity methods is widely over costly, a significant part of the computations resulting in fully negligible contributions.

In standard flux formulations, it is difficult to quantify the relative importance of the various contributions to the local heating rates because the individual contributions are not identified as such in the formalism. Green (1967) suggested that a reformulation of radiative transfers in terms of net exchanges allows quantifying the relative importance of physically distinct contributions to the local heating rates and could help design more efficient models. In Green's approach, called here the Net Exchange Formulation (NEF), the quantity under consideration is directly the net energy exchanged between two atmospheric layers (or more generally two surfaces or gas volumes). Joseph and Bursztyn (1976) attempted to use the net exchange approach to compute radiative exchanges in the terrestrial atmosphere. Despite some numerical difficulties, they showed that radiative net exchanges between an atmospheric layer and boundaries (space and ground) are dominant although the net exchanges with the rest of the atmosphere are not negligible as they contribute to approximatively 15% of the total energy budget. With NEF, Bresser et al. (1995) did elaborate analytical developments for particular cases in order to compute the radiative damping of gravity waves. The well known Curtis matrix ((Curtis, 1956), see for instance,[]Goody.Yung-1989) may be related to NEF, but in the Curtis matrix approach one way exchanges are considered instead of net exchanges, which means that useful properties of NEF, such as the strict simultaneous satisfaction of energy conservation and reciprocity principle, are abandoned. Fels and Schwarzkopf (1975) and Schwarzkopf and Fels (1991) take advantage of the importance of the cooling to space to develop an accurate and rapid longwave radiative code. They don't use the NEF but their work may be easily understand in the net exchange framework.

Similar developments were also motivated by various engineering applications. Hottel's method (Hottel and Sarofim, 1967), also named the zone method, is originally based on NEF. However, difficulties were encountered considering multiple reflection configurations and the NEF symmetry was practically abandoned. Cherkaoui et al. (1996, 1998), Dufresne et al. (1998) and De Lataillade et al. (2002) showed that NEF can be used to derive efficient Monte Carlo algorithms. Dufresne et al. (1999) used NEF to identify and analyze dominating spectral ranges, emphasizing the contrasted behav-

ior of gas-gas and gas-surfaces exchanges. Finally, this formulation was recently used to analyze longwave radiative exchanges on Earth with a Monte-Carlo method (Eymet et al., 2004).

In the present paper, we show how NEF can help derive efficient operational radiative codes for circulation models. This code is now operational in the general circulation model developed jointly by Laboratoire de Météorologie Dynamique and the University of Oxford (Forget et al., 1999). As an example, this circulation model has been used to produce a climate database for Mars for the European Space Agency [1] (Lewis et al., 1999). In Sec. 2 the NEF is presented in the specific case of stratified atmospheres and analysis are performed for typical Martian conditions. Section 3 discusses the questions related to operational radiative code derivations, in particular those related to vertical integration procedures and reflections at the surface. The time integration scheme is considered in Sec. 4, first by investigating the numerical instabilities that may occur in the high atmosphere, then by finding how computer time may be saved without loosing accuracy. Summary and conclusions are in section 5.

2 Net exchange formulation

2.1 General approach

Longwave atmospheric radiative codes are generally based on flux formulations. Angular integration of all intensities at each location leads to the radiative flux field, $\vec{q_R}$, the divergence of which gives the radiative budget of an elementary volume dV_M around point M as

$$d\mathcal{Q} = -div\,(\vec{q_R})\,dV_M \tag{1}$$

In an exchange formulation, the volumic radiative budgets are addressed directly without explicit formulation of the radiative intensity and radiative flux fields. Corresponding formulations include complex spectral and optico-geometric integrals that may come down to (Dufresne et al., 1998)

$$d\mathcal{Q} = dV_M \int_0^{+\infty} d\nu \int_{\mathcal{A}} dV_P \int_{\Gamma_{M,P}} d\gamma \quad \tau_\gamma^\nu K_M^\nu K_{P,\gamma}^\nu \left(B_P^\nu - B_M^\nu\right) \tag{2}$$

[1] The database is accessible both with a Fortran interface for engineering and through the WEB at **http://www.lmd.jussieu.fr/mars.html**

In this expression, ν is the frequence, $\mathcal{A}$ represents the entire system (for an atmosphere, the entire atmosphere plus ground and space boundaries), $\Gamma_{M,P}$ is the space of all optical paths joining locations M and P. For each optical path γ, τ_γ^ν is the spectral transmission function along the path. B_P^ν and B_M^ν are the spectral blackbody intensities at the local temperatures of P and M, and K_M^ν is the absorption coefficient in M. The differential dV_P around location P is either an elementary volume or an elementary surface and $K_{P,\gamma}^\nu$ is either the absorption coefficient in P (if P is within the atmosphere) or the directional emissivity (if P is at the boundaries).

Expressed this way, the radiative budget of elementary volume dV_M can be seen as the difference of two terms: the radiative power absorbed by dV_M coming from the whole atmosphere plus surface and space (B_P part of Eq. 2) minus the power emitted by dV_M toward all other locations (B_M term). When separated this way, the equation can be simplified further noticing that the B_M part (total emission of volume dV_M) reduces to $4\pi \int_0^{+\infty} K_M^\nu B_M^\nu d\nu$. This approach is the current basis for engineering zone method and Curtis matrix (see for instance, Goody and Yung, 1989).

In NEF, equation 2 is rather interpreted keeping the formal symmetry as the sum of the individual net exchanges between volume dV_M and all other elementary volumes or surfaces (including space in the case of an atmosphere). An individual spectral net exchange rate between dV_M and dV_P

$$\psi^\nu(dV_M, dV_P) = dV_M dV_P \int_{\Gamma_{M,P}} d\gamma \quad \tau_\gamma^\nu K_M^\nu K_{P,\gamma}^\nu \left(B_P^\nu - B_M^\nu\right) \tag{3}$$

is just the power emitted by dV_P and absorbed by dV_M minus that emitted by dV_M and absorbed by dV_P. For a discretized atmosphere, the spectral net exchange rate between two meshes i and j reads:

$$\psi_{i,j}^\nu = \int_{\mathcal{A}_i} \int_{\mathcal{A}_j} \psi^\nu(dV_M, dV_P) \tag{4}$$

where $\mathcal{A}_i$ and $\mathcal{A}_j$ are the volumes or surfaces of meshes i and j. The spectral radiative budget ψ_i^ν of mesh i is the sum of the net exchange rates between i and all other meshes j:

$$\psi_i^\nu = \sum_j \psi_{i,j}^\nu \tag{5}$$

A very specific feature of this formulation lies in the fact that both the reciprocity principle, the energy conservation principle and the second thermodynamic principle may be strictly satisfied whatever the level of approximation is retained to solve Eq. 3 and 4. The reciprocity principle states that the light path does not depend on the direction in which light propagates, which means that the integrals of the optical transmission τ_γ^ν over both the optical path space $\Gamma_{M,P}$ and over the reciprocal space $\Gamma_{P,M}$ are the same:

$$\int_{\Gamma_{M,P}} d\gamma \tau_\gamma^\nu = \int_{\Gamma_{P,M}} d\gamma \tau_\gamma^\nu \tag{6}$$

Using Eq. 3, the reciprocity principle reduces to $\psi^\nu(dV_M, dV_P) = -\psi^\nu(dV_P, dV_M)$. This condition may be satisfied provided that the same computation is used for both $\psi^\nu(dV_M, dV_P)$ and $-\psi^\nu(dV_P, dV_M)$. In other words, when photons emitted by dV_M and absorbed by dV_P are counted as an energy loss for volume dV_M, the same approximate energy amount is counted as an energy gain for dV_P. As a direct consequence, the energy conservation principle is also satisfied. Finally, provided that the difference $(B_P^\nu - B_M^\nu)$ that appears as such inside the optical path integral is preserved, Eq. 3 ensures that warmer regions heat colder regions in accordance with the second thermodynamic principle.

Altogether, the NEF allows the derivation of approximate numerical schemes strictly satisfying both the reciprocity principle, the energy conservation principle and the second thermodynamic principle. Any approximation may be retained for the integration over the optical path domain without any risk of inducing artificial global energy sources, or non physical energy redistributions.

2.2 Application to the CO_2 band 15μm in the Martian context

After these general considerations, we illustrate the net exchange approach in the case of the CO_2 15μm band on Mars. At this first stage, we make the following simplifying assumptions:

- the atmosphere is perfectly stratified along the horizontal (plan parallel assumption).
- the surface is treated as a black-body (emissivity ϵ=1).
- the atmosphere is assumed dust free.

Under these assumptions, the space of relevant optical paths reduces to straight lines between exchange positions. Dividing the atmosphere into N layers, spectral net exchange $\psi_{i,j}^\nu$ between layer i and layer j can be derived from Eq. 3 and 4 as

$$\begin{aligned}\psi_{i,j}^\nu = &\int_{Z_{i-\frac{1}{2}}}^{Z_{i+\frac{1}{2}}} \int_{Z_{j-\frac{1}{2}}}^{Z_{j+\frac{1}{2}}} \int_0^{\frac{\pi}{2}} \\ &2(B_{z_j}^\nu - B_{z_i}^\nu) k^\nu(z_i)\rho(z_i) k^\nu(z_j)\rho(z_j) \\ &\exp\left(-\left|\int_{z_i}^{z_j} \frac{k^\nu(z)\rho(z)}{\cos\theta} dz\right|\right) \tan\theta \\ &d\theta dz_i dz_j\end{aligned} \tag{7}$$

where $Z_{i-\frac{1}{2}}$ and $Z_{i+\frac{1}{2}}$ are the altitudes at the lower and higher boundaries of atmospheric layer i, ρ is the gas density, k^ν is the spectral absorption coefficient and θ is the zenith angle. The previous equation may be rewritten as:

$$\begin{aligned}\psi_{i,j}^\nu = &\int_{Z_{i-\frac{1}{2}}}^{Z_{i+\frac{1}{2}}} \int_{Z_{j-\frac{1}{2}}}^{Z_{j+\frac{1}{2}}} \\ &(B_{z_j}^\nu - B_{z_i}^\nu) \left|\frac{\partial^2 \Upsilon^\nu(z_i, z_j)}{\partial z_i \partial z_j}\right| dz_i dz_j\end{aligned} \tag{8}$$

where Υ^ν is the spectral integrated transmission function defined as

$$\begin{aligned}\Upsilon^\nu(z, z') = &2\int_0^{\frac{\pi}{2}} \\ &\exp\left(-\left|\int_z^{z'} \frac{k^\nu(x)\rho(x)}{\cos\theta} dx\right|\right) \sin\theta \ \cos\theta \ d\theta\end{aligned} \tag{9}$$

With the same assumptions, the spectral net exchange rate $\psi_{i,b}^\nu$ between layer i and ground or space can be derived from Eq. 3 as

$$\begin{aligned}\psi_{i,b}^\nu = &\int_{Z_{i-\frac{1}{2}}}^{Z_{i+\frac{1}{2}}} \int_0^{\frac{\pi}{2}} \\ &2(B^\nu(T_b) - B_{z_i}^\nu) k^\nu(z_i)\rho(z_i) \\ &\exp\left(-\left|\int_{z_i}^{z_b} \frac{k^\nu(z)\rho(z)}{\cos\theta} dz\right|\right) \sin\theta \ d\theta dz_i\end{aligned} \tag{10}$$

with $T_b = T_s$ for exchanges with the planetary surface (at temperature T_s) and $T_b = 0$ K for cooling to space. This equation may be rewritten as:

$$\psi_{i,b}^\nu = \int_{Z_{i-\frac{1}{2}}}^{Z_{i+\frac{1}{2}}} (B^\nu(T_b) - B_{z_i}^\nu) \left|\frac{\partial \Upsilon^\nu(z_i, z_b)}{\partial z_i}\right| dz_i \tag{11}$$

This last equation is well known as it is commonly used to compute the cooling to space.

In practice, net exchange computations require therefore angular, spectral and vertical integrations. In the present study, the following choices are made:

1. As in most GCM radiative codes, the angular integration is computed by applying the diffusive approximation which consists in the use of a mean angle $\overline{\theta}$ ($1/\cos\overline{\theta} = 1.66$, see Elsasser, 1942).

2. As in the original martian model, the spectral integration is replaced by a band model approach in which the Planck functions and wide band transmitivities are separated (Morcrette et al., 1986; Hourdin, 1992). [2]

3. The vertical integration is what we concentrate on in Section 3 with various levels of approximation.

With the diffusive approximation and the use of wide band transmitivities, the net exchange $\psi_{i,j}$ becomes after spectral integration of Eq. 8 over wide bands m:

$$\psi_{i,j} = \int_{Z_{i-\frac{1}{2}}}^{Z_{i+\frac{1}{2}}} \int_{Z_{j-\frac{1}{2}}}^{Z_{j+\frac{1}{2}}} \sum_m (\bar{B}^m_{z_j} - \bar{B}^m_{z_i}) \overline{\xi}^m_{z_i,z_j} \Delta\nu_m dz_i dz_j \quad (12)$$

with

$$\overline{\xi}^m_{z_i,z_j} = \left| \frac{\partial^2 \bar{\tau}^m(z_i,z_j)}{\partial z_i \partial z_j} \right| \quad (13)$$

where $\bar{\tau}^m(z_i,z_j)$ is the wide band transmitivity between z_i and z_j with a mean angle $\overline{\theta}$ and $\Delta\nu_m$ is the band width.

The net exchange $\psi_{i,b}$ between layer i and boundary b (ground or space) becomes after spectral integration of Eq. 11:

$$\psi_{i,b} = \int_{Z_{i-\frac{1}{2}}}^{Z_{i+\frac{1}{2}}} \sum_m \left(\bar{B}^m(T_b) - \bar{B}^m_{z_i}\right) \overline{\xi}^m_{z_i,z_b} \Delta\nu_m dz_i \quad (14)$$

with

$$\overline{\xi}^m_{z_i,z_b} = \left| \frac{\partial \bar{\tau}^m(z_i,z_b)}{\partial z_i} \right| \quad (15)$$

Finally the net exchange $\psi_{s,e}$ between the ground surface s and space e becomes:

$$\psi_{s,e} = \sum_m -\bar{B}^m(T_s) \overline{\xi}^m_{z_s,z_e} \Delta\nu_m \quad (16)$$

with

$$\overline{\xi}^m_{z_s,z_e} = \bar{\tau}^m(z_s,z_e) \quad (17)$$

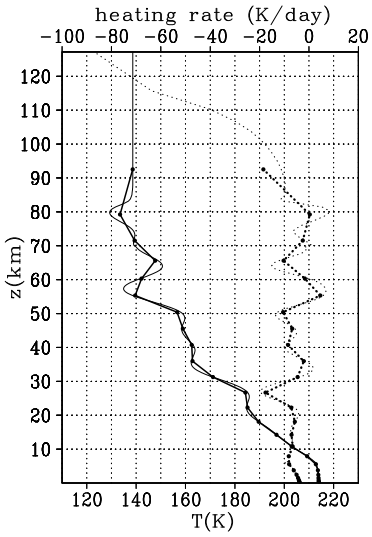

Figure 1: Temperature vertical profile (K, bottom axis, continuous line) with 500 layers (thin line) and 25 layers (bullet, thick line). Each temperature of the 25 layers grid is the mean of 20 layers of the high resolution grid (finite volume representation). The reference heating rate (K/day, top axis, dotted line) is also displayed for the two grids.

2.3 Reference case

We first present a computation of net exchanges on a typical 25 layers GCM grid (Table 1), with refined discretization near the surface. To avoid problems with the vertical integration for this reference computation, exchanges are first computed on an over-discretized grid of 500 layers (Fig. 1), each layer of the coarse GCM grid corresponding exactly to 20 layers of the 500 layers grid. An exchange between two atmospheric layers of the coarse grid is simply obtained as the sum of the 20x20 exchanges from the finer grid.

[2] This approach is exact for a spectral interval narrow enough to use a constant value of the Planck function. For larger intervals, temperature variations affect the correlation between the gaz absorbtion spectrum and the Planck function. Following Morcrette et al. (1986), this effect was accounted for in the original model by using different sets of fitting parameters for the transmission function depending upon the temperature of the emitting layers. Here, we only use one set of parameters and control tests indicated that this simplification has a negligible effect on the estimated radiative heat sources.

We use a reference temperature profile (Fig. 1) derived from the measurement taken by two Viking probes during their entry in the Martian atmosphere (Seiff, 1982) and already used by Hourdin (1992). In the upper atmosphere, there is no systematic temperature increase as there is no significant solar radiation absorption equivalent to that the ozone layer on Earth. In the middle atmosphere, gravity waves and thermal tides disrupt the temperature profile. Near the surface, the quasi isothermal part of this averaged profile hides a strong diurnal cycle. The surface pressure is fixed to 700 Pa.

2.4 Net exchange matrix

NEF offers a meaningful matrix representation of radiative exchanges. A graphical example of such a matrix is shown in Fig. 2. Each element displays the net exchange rate $\chi_{i,j}$ for a given pair i, j of meshes converted in terms of heating rate:

$$\chi_{i,j} = \frac{g}{Cp}\frac{1}{\delta t}\frac{\psi_{i,j}}{\delta p_i} \tag{18}$$

where g is the gravity, Cp the gas mass heat capacity, and δt the length of the Martian day ($\delta t = 88775s$). For the ground , the heating rate is arbitrary computed using a thermal capacitance of 1 $J.K^{-1}.m^{-2}.day^{-1}$. The total heating rate of a layer i is:

$$\chi_i = \sum_j \chi_{i,j}. \tag{19}$$

$\chi_{i,j}$ and $\chi_{j,i}$ are of opposite sign but the exchange matrices expressed in K/day are not antisymmetric as they would be if expressed in W/m^2 ($\psi_{i,j} = -\psi_{j,i}$ but $\chi_{i,j} \neq -\chi_{j,i}$).

2.4.1 Matrix characteristics

As an example of reading Fig. 2, consider layer $i = 10$ (marked in the figure). The temperature profile and total heating rate χ_i are also plotted on both sides. The horizontal line of the matrix shows the decomposition of the heating rate in terms of net exchange contributions (see Eq. 19). This partitioning of the heating rates first emphasizes some well established physical pictures. The cooling to space is the dominant part of the heating rate: it essentially defines the general form and the order of magnitude of the heating rate vertical profile. This well known property has been widely used to derive approximate solutions in atmospheric context (e.g. Rodgers and Walshaw, 1966; Fels and Schwarzkopf, 1975; Schwarzkopf and Fels, 1991). Internal exchanges within the atmosphere are by far dominated by the exchanges with adjacent layers (note that there is a factor of ≈ 3 between two consecutive colors). As a consequence, the net exchange matrix is very sparse. A very few terms dominate all the others. These important terms are the exchanges with boundaries (space and surface) and the exchanges with adjacent layers. Thanks to the NEF, the relative magnitude of these terms can be quantified.

2.4.2 Thermal aspects

In each spectral band, each contribution $\overline{\chi}^m_{i,j}$ to the total net exchange rate $\chi_{i,j}$ is the integral of the product of two terms: the blackbody intensity difference between z_i and z_j and the optical exchange factor $\overline{\xi}^m_{z_i,z_j}$ (e.g. Eq. 12). The sign of the net exchange rate $\overline{\chi}^m_{i,j}$ only depends on the temperature difference between i and j as the optical exchange factor $\overline{\xi}^m_{z_i,z_j}$ is always positive. Layer i heats layer j only if its temperature T_i is greater than T_j. The direct influence of the temperature profile on the exchange matrix can be seen on Fig. 2. For instance layer 10 is heated by the warmer underlying atmosphere and surface and looses energy toward the colder layers above and toward space. The picture is more complex in the upper atmosphere where strong temperature variations are generated by atmospheric waves. In this region, a layer can be heated by both adjacent warmer layers (e.g. layer 20). In particular these radiative exchange between adjacent layers are known to damp the possible temperature oscillations due to atmospheric waves (Bresser et al., 1995).

Finally, the gas radiative properties depend much less on the temperature than the black body intensity. Therefore the metric of optical exchange factors $\overline{\xi}$ may be assumed as constant for qualitative exchange analysis, and even to some extent for practical computations as discussed later on.

2.4.3 Spectral aspects

The exchange factors $\overline{\xi}$ between two meshes are proportional to the gas transmission $\bar{\tau}$ for the exchange between surface and space (Eq. 17), proportional to the first derivative of $\bar{\tau}$ for the

Layer #	σ	Approx. height (m)	Layer #	σ	Approx. height (km)	Layer #	σ	Approx. height (km)
1	0.99991	3.6	10	0.9251	3.030	19	0.3256	43.69
2	0.99958	16.4	11	0.8787	5.037	20	0.2783	49.80
3	0.99898	39.8	12	0.8157	7.934	21	0.2359	56.24
4	0.99789	82.1	13	0.7403	11.70	22	0.1975	63.15
5	0.99592	159.0	14	0.6597	16.19	23	0.1613	71.04
6	0.99238	297.9	15	0.5803	21.19	24	0.1275	80.21
7	0.98605	547.0	16	0.5061	26.52	25	0.0842	96.35
8	0.97494	988.4	17	0.4388	32.07			
9	0.95598	1753	18	0.3788	37.80			

Table 1: Low resolution (i.e. 25 layers) vertical grid characteristics: layer number, σ levels ($\sigma = P/P_s$, with P_s the surface pressure) and approximate corresponding heights.

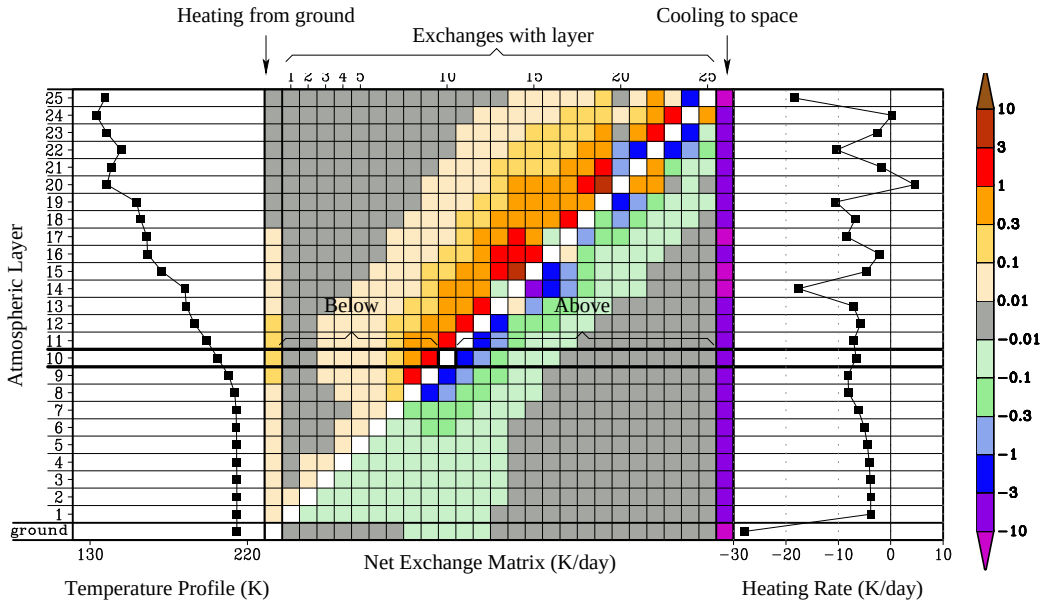

Figure 2: Graphical representation of radiative net exchange rates in the Martian atmosphere. Left: temperature profile, Middle: net exchange matrix, Right: heating rate. The vertical axis is the layer number. Same conditions as in Fig. 1.

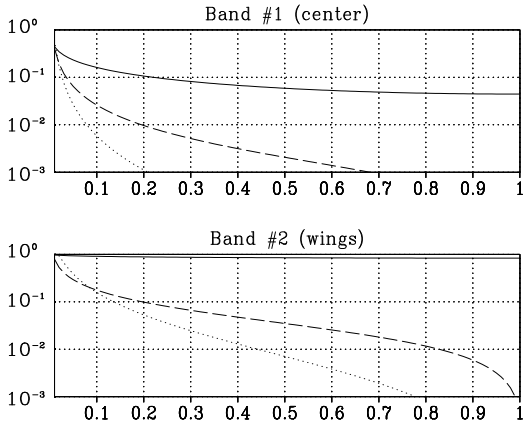

Figure 3: Gas transmission τ (solid) and its two first derivatives normalized by the emissivity $\bar{\epsilon}$ of the gas layer, $1/\bar{\epsilon}.|\partial\bar{\tau}/\partial X|$ (dash) and $1/\bar{\epsilon}^2.|\partial^2\bar{\tau}/\partial X^2|$ (dot), as a function of the normalized integrated mass of atmosphere $X = (P - P_s)/P_s$, for the central part (band #1, upper plot) and for the wings part (band #2, lower plot) of the CO_2 $15\mu m$ band. The atmospheric temperature is assumed uniform ($T = 200K$) and the surface pressure is $P_s = 700Pa$.

exchanges between a layer and surface or space (Eq. 15) and proportional to the second derivative of $\bar{\tau}$ for the exchanges between two atmospheric layers (Eq. 13). The behavior of optical exchange factors can be understood by analyzing these three functions. To allow comparison, we normalize them by the product of the emissivity at both extremities. If the extremity i is a gas layer of differential thickness dz_i, the emissivity is:

$$\bar{\epsilon}^m_{z_i} = dz_i \int_\nu k^\nu(z_i)\rho(z_i)d\nu \qquad (20)$$

If the extremity i is ground or space, $\bar{\epsilon}^m_i = 1$. We also use a normalized integrated mass X of atmosphere

$$X(z) = \frac{g}{P_s}\int_s^z \rho dz' \qquad (21)$$

where P_s is the ground pressure.

The wide band model used in this study has two spectral bands chosen empirically (Hourdin, 1992). The first one (band #1), ranging from 635 to 705 cm^{-1}, corresponds to the central part of the CO_2 15 μm band. The second one (band #2), ranging from 500 to 635 cm^{-1} and from 705 to 865 cm^{-1} corresponds to the wings. The three normalized functions, $\bar{\tau}$, $1/\bar{\epsilon}_{z_i}.\partial\bar{\tau}/\partial X$ and $1/(\bar{\epsilon}_{z_i}.\bar{\epsilon}_{z_j}).\partial^2\bar{\tau}/\partial X^2$, that may also be seen as normalized exchange factors, are displayed in Fig. 3 for the two bands. The three normalized exchange factors go to 1 when X goes to 0. Indeed, when the two extremities are adjacent, the exchange factor is the product of the emissivity at both extremities[3].

When X increases, the normalized exchange factor slowly decreases (in particular for band #2) if the two extremities are black surfaces (here space and ground); it decreases faster if one extremity is a gas layer and decreases even faster if the two extremities are gas layers (Fig. 3). This is an illustration of the so-called "spectral correlation effect" (e.g. Zhang et al., 1988; Modest, 1992; Dufresne et al., 1999). For the exchange between two gas layers, both absorption and emission are maximum in spectral regions near the center of the absorbing lines. But exactly at the same frequencies gas absorption creates a strong decrease of the transmission when the distance between extremities increases. Thus the exchange strongly decreases with distance. On the contrary, the exchange between ground and space is most important in spectral regions where the spectral transmission is high, that is where the gas absorption is low. Thus the exchange factor between ground and space is much less sensitive to the integrated air mass between them. Exchange between a layer and ground or space is an intermediate case.

When X increases, the decrease of the three normalized exchange factors is faster for the central part of the CO_2band (band #1) than for the wings (band #2) (Fig. 3). As a consequence, the decrease with distance of the exchange between two atmospheric layers is more important in band #1 (left panel of Fig. 4) than in band #2 (right panel of Fig. 4). The exchanges between adjacent layers are much greater for band #1 than for band #2, whereas distant exchanges have the same magnitude for the two bands. For the cooling to space, the competition between the decrease of $|\partial\bar{\tau}/\partial X|$ and the increase of the local black body intensity yields noticeably different vertical profiles: The absolute value of the cooling to space decreases when the layer is closer to the surface for band #1 whereas it increases for band #2.

[3]This is only true in the limit where the gas layer(s) is(are) optically thin. In the example presented here, the emissivities are computed for layers with a normalized thickness $\Delta X = 0.01$.

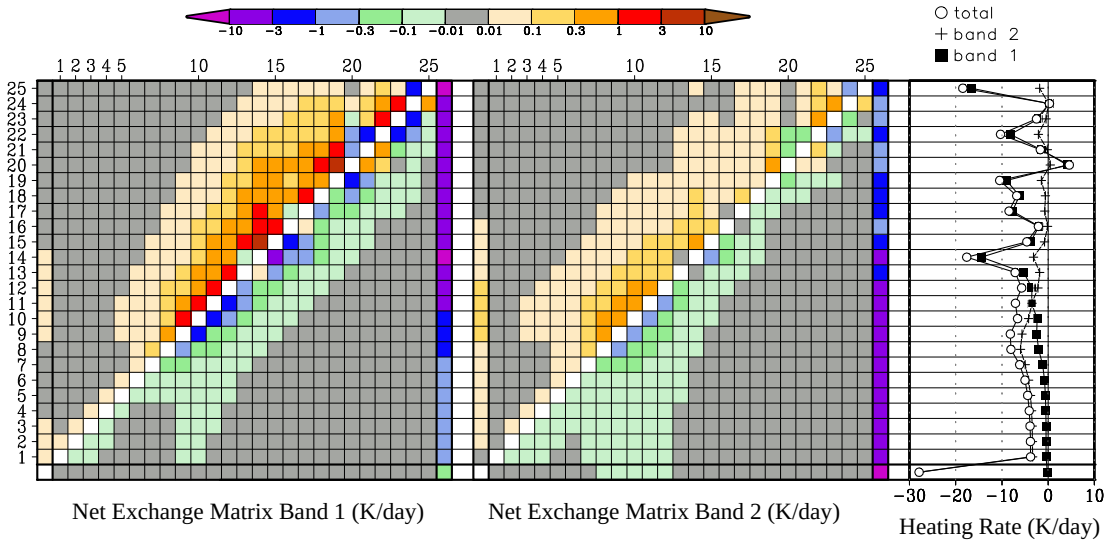

Figure 4: Graphical representation of the net exchange matrix for spectral bands # 1 (left) and # 2 (middle). Same conditions as in Fig. 2. On the right side, the total heating rate is shown for band # 1 (black squares), for band # 2 (crosses) and over the whole spectrum (open circles).

3 Vertical integration

In the above reference computation, net exchanges have been computed using given sub-grid scale temperature profiles(Fig. 1). In practice, with circulation models, only mean temperatures are known for each layer[4] and assumptions are required concerning sub-grid scale profiles. First we present the very simple assumption of a uniform temperature within each atmospheric layer. This allows us to highlight the link between NEF and flux formulations. Then we address the more general case of non isothermal layers and finally we highlight the modifications that are required in the case of a reflective surface.

3.1 Isothermal layers

For isothermal layers, the individual exchanges contributing to the radiative budget of layer i ($\psi_i = \sum_j \psi_{i,j}$) take a simple form (Eq. 12 and 13) reducing to

$$\psi_{i,j} = \sum_m \overline{\xi}^m_{i,j} (\bar{B}^m_j - \bar{B}^m_i) \tag{22}$$

with

$$\overline{\xi}^m_{i,j} = \left| \bar{\tau}^m_{i+\frac{1}{2},j-\frac{1}{2}} - \bar{\tau}^m_{i-\frac{1}{2},j-\frac{1}{2}} - \bar{\tau}^m_{i+\frac{1}{2},j+\frac{1}{2}} + \bar{\tau}^m_{i-\frac{1}{2},j+\frac{1}{2}} \right| \tag{23}$$

In the equivalent flux formulation, the individual contributions of the radiation emitted by layer i to the flux at interface $j+\frac{1}{2}$

$$F_{i\to j+\frac{1}{2}} = \sum_m \bar{B}^m_i \left(\bar{\tau}^m_{i+\frac{1}{2},j+\frac{1}{2}} - \bar{\tau}^m_{i-\frac{1}{2},j+\frac{1}{2}} \right) \tag{24}$$

are first summed over i to compute the radiative flux $F_{j+\frac{1}{2}}$ at each interface $j+\frac{1}{2}$. The radiative budget of each layer j then reads:

$$\begin{aligned} \psi_j &= F_{j-\frac{1}{2}} - F_{j+\frac{1}{2}} \\ &= \sum_i F_{i\to j-\frac{1}{2}} - \sum_i F_{i\to j+\frac{1}{2}} \end{aligned} \tag{25}$$

An exact equivalence between the net exchange and flux formulations is obtained by noting that

$$\psi_{i,j} = \left| F_{j\to i+\frac{1}{2}} - F_{j\to i-\frac{1}{2}} \right| - \left| F_{i\to j+\frac{1}{2}} - F_{i\to j-\frac{1}{2}} \right| \tag{26}$$

and using the property $\bar{\tau}_{i,j} = \bar{\tau}_{j,i}$.

For developing a radiative code, NEF however presents advantages. With flux formulation, fluxes are first integrated over altitude z and then differentiated. When temperature contrasts are weak (here near the surface for instance), net exchange rates can be by orders of

[4] We assume that circulation models make use of finite volume representations and that GCM outputs are representative of mean temperatures rather than mid-layer temperatures

magnitude smaller than fluxes. Computing first the fluxes and then the differences may lead to strong accuracy loss which we observed could induce reciprocity principle violations (colder layers heating warmer layers for instance)[5].

In Fig. 5, we show the error on net exchanges if the isothermal approach is retained for all exchanges with respect to the reference 500-layer simulation. The error is very large around the diagonal and often larger than the exchange itself. Indeed, at frequencies where significant CO_2 emission occurs (close to absorption lines centers) the atmosphere is extremely opaque, which means that most emitted photons have very short path lengths compared to layer thicknesses. Consequently, exchanges between adjacent layers are mainly due to photon exchanged in the immediate vicinity of the layer interface. In this thin region, temperature contrasts are much weaker than the differences between mean layer temperatures. The isothermal approximation thus results in a strong overestimation of the net exchanges.

The relative error due to the isothermal hypothesis strongly decreases with distance between layers. This feature is further commented in appendix.

3.2 Net exchanges between adjacent layers

The specific difficulty of exchange estimations in the case of adjacent layers is commonly identified and solutions have been implemented in flux computation algorithms (e.g. Morcrette et al., 1986). In most GCMs, only the average layer temperatures and compositions are available. Here a linear approximation is retained for B to describe the atmosphere close to the mesh interface. Because of the symmetry of Eq. 8 in z_i and z_j, the linear approximation is strictly equivalent to a quadratic approximation in the limit case of two layers of identical thicknesses (see Appendix). When computing $\psi_{i,i+1}$ we therefore assume that $B(z)$ is linear between $z_{i-1/2}$ and $z_{i+3/2}$, satisfying the following constraints for $j = i \pm 1$ (Fig. 6):

$$\int_{Z_{j-1/2}}^{Z_{j+1/2}} B(z)dz = B_j.\Delta z_j \qquad (27)$$

[5]This problem may be partially overcome in the flux formulation by introducing the blackbody differential fluxes $\tilde{F} = \pi B - F$ (e.g. Ritter and Geleyn (1992))

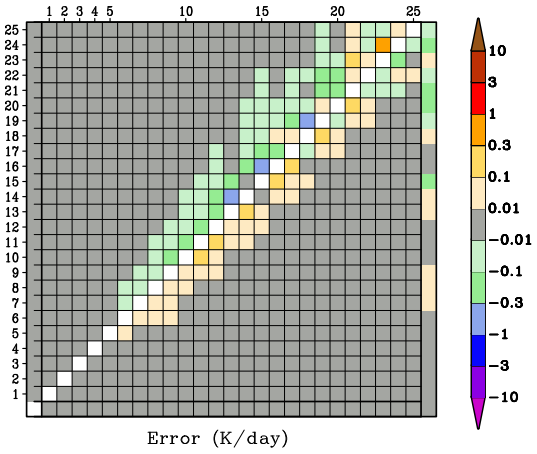

Figure 5: Error matrix with the isothermal layer assumption. Line i column j gives the error in K/day for the heating rate of layer i due to its exchange with layer j. The error is computed with respect to the reference computation performed with 20 sub-layers inside each layer. Other conditions are the same as in Fig. 2.

Note that in this approach, the assumed temperature profile inside a layer is different when computing the exchange with the layer just above or just below.

With this assumption, exact integration procedures could be designed, for instance using the analytical solution available for the best fitted Malkmus transmission function (Dufresne et al., 1999), or integrating by parts and tabulating integrated transmission function from line by line computations. Here we test a more basic solution by dividing the linear profile into isothermal sub-layers, with thiner sub-layers closer to the interface (Fig. 6). The sub-discretization scheme was tested against reference simulations. For the present application, a satisfactory accuracy is reached with a sub-discretization into three isothermal sub-layers of increasing thicknesses ($\Delta z/7$, $2\Delta z/7$ and $4\Delta z/7$) away from the interface.

Whatever the integration procedure, a direct consequence of the previous linear black body intensity assumption is that the net exchange between two adjacent layers may be still written formally like the net exchange between isothermal layers (Eq. 22). Only the expression of the exchange coefficient $\overline{\xi}^m_{i,i\pm1}$ depends on the temperature profile hypothesis.

We finally adopt the following solution

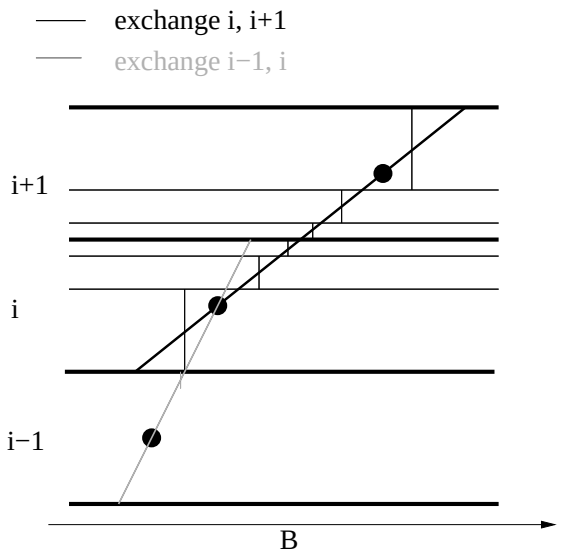

Figure 6: A linear black body intensity profile approximation is used for computation of the net exchanges between adjacent layers. The black body intensity profile inside a layer is different when computing the exchange with the layer just above (black line) or just below (grey line). The sub-grid discretization is also shown (thin lines).

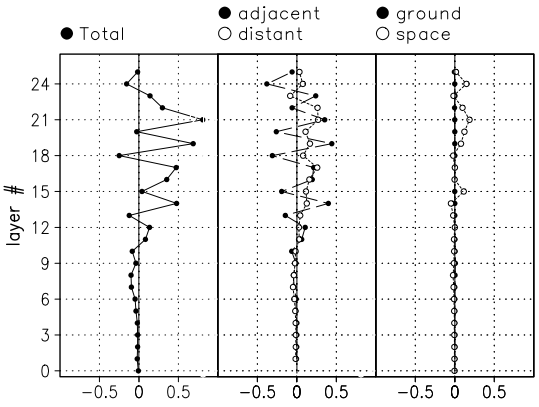

Figure 7: Vertical profile of the heating rate error in K/day due to the vertical integration scheme (left), and part of this error due to the computation of the net exchange with adjacent layers (middle, square), with distant layers (middle, circle), with ground (right, square) and with space (right, circle). The error is computed with respect to the reference computation performed with 20 sub-layers inside each layer. Other conditions are the same as in Fig. 2. The vertical axis is the layer number.

for the vertical integration: the above sub-discretization into three isothermal sub-layers is used to compute the radiative exchanges between adjacent layers whereas the simple isothermal layer assumption is used to compute the exchange between distant layers. For the exchange between ground and first layer, we assume the temperature of gas just above the surface to be $T_0 = (T_1+T_s)/2$ and a linear B profile between T_1 and T_0. An isothermal description is retained for the exchange between the optically thin upper layer and space. The global error due to the vertical integration scheme as well as the origin of the error are displayed Fig. 7. The analytical expression of these errors are presented in appendix for some cases. One should have in mind that results are compared with a high resolution vertical grid where the temperature profile has a more precise description than in the low resolution grid.

3.3 Exchanges with reflection at the surface

The above presentation assumes that the surface behaves as a black-body. In practice, surface emissivity can differ from 1. The mean emissivity of the Martian surface is believed to be of the order of 0.95 (Santee and Crisp, 1993), and emissivity is believed to be lower in some regions (Forget et al., 1995).

When reflection at the surface is present, two atmospheric layers can exchange photons, either directly, or through reflection at the surface. For instance, the net exchange between two atmospheric layers i and j (Eq. 12) becomes:

$$\psi_{i,j} = \int_{Z_{i-\frac{1}{2}}}^{Z_{i+\frac{1}{2}}} \int_{Z_{j-\frac{1}{2}}}^{Z_{j+\frac{1}{2}}} \sum_m (\bar{B}^m_{z_j} - \bar{B}^m_{z_i}) \left[\overline{\xi}^m_d(z_i, z_j) + \overline{\xi}^m_s(z_i, z_j)\right] dz_i dz_j \quad (28)$$

where $\overline{\xi}^m_d$ is the optical exchange factor for direct exchanges

$$\overline{\xi}_d(z_i, z_j) = \left| \frac{\partial^2 \overline{\tau}(z_i, z_j)}{\partial z_i \partial z_j} \right| \quad (29)$$

and $\overline{\xi}^m_s$ the optical exchange factor through reflection at the surface:

$$\overline{\xi}_s(z_i, z_j) = (1 - \overline{\epsilon_s}) \left| \frac{\partial^2 \overline{\Gamma_s}(z_i, z_j)}{\partial z_i \partial z_j} \right| \quad (30)$$

where $\bar{\epsilon_s}$ is the surface emissivity and $\overline{\Gamma_s}(z_i, z_j)$ is the transmission function from z_i to z_j via the surface for a spectral interval. Assuming the diffusive approximation this transmission writes:

$$\overline{\Gamma_s}(z_i, z_j) = \int_\nu (\tau^\nu(z_i, 0)\tau^\nu(0, z_j))\, d\nu \quad (31)$$

In the original flux formulation, as well as in other radiative codes based on the so-called absorbtivity/emissivity method, the downward flux is first integrated from the top of the atmosphere to the surface. The reflected part of this downward flux is then added to the flux emitted by the grey surface. This flux is then used as a limit condition to integrate the upward flux up to the atmospheric top. This assumption corresponds to the following approximation :

$$\overline{\Gamma_s}(z_i, z_j) \approx \overline{\tau}(z_i, 0)\overline{\tau}(0, z_j) \quad (32)$$

which is wrong for wide and narrow band models because the spectral information is forgotten at the surface. The error on the heating rate is particularly strong for the layers near the surface. For a surface emissivity of 0.9, as expected, the exact solution displays small changes in the heating rate compare to the case where the surface is black (plus signs and circles in the left on Fig. 8). On the other side, the computation which neglects the spectral correlation at the surface (squares) displays a very large and unrealistic change of the heating rate near the surface.

A useful property can be used to check the results with a reflective surface. Let us consider an atmosphere with a thin layer near the surface having the same temperature as the surface itself. This layer will never exchange energy with the surface because both are at the same temperature. If the surface emissivity differs from 1, the exchange of this layer with the atmosphere above and with the space will be increased through reflection at the surface. For an optically thin layer and for a perfect mirror ($\epsilon = 0$) all those exchanges, and hence the radiative cooling, will be exactly twice that without reflection ($\epsilon = 1$) (Cherkaoui et al., 1998). The net exchange computation fulfills this property (plus signs and circles in the right hand of Fig. 8) but the original flux model does not (square).

The above computations were performed with a prescribed vertical temperature profile. In order to evaluate the error associated to incorrect treatment of reflection when all the physical processes (radiation, turbulent vertical mixing...) are active, we present hereafter results obtained with a 1D model that corresponds to a single vertical column of the 3D GCM.

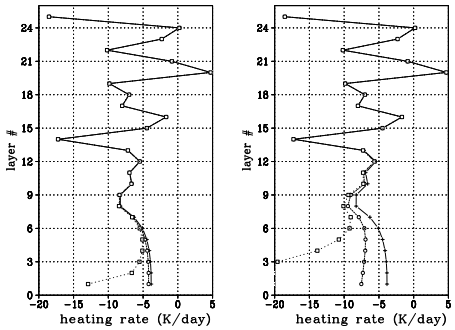

Figure 8: **Left:** Vertical profile of the heating rate when the surface is perfectly black (cross, continuous line) and when the surface has an emissivity $\epsilon_s = 0.9$, the computation being either exact (circle, dash line) or neglecting spectral correlation when reflection at the surface occurs (square, dotted line). Same atmospheric conditions as in Fig. 1. The vertical axis is the layers number. **Right:** Same, but with a perfectly reflecting surface ($\epsilon_s = 0$).

When the temperature profile is prescribed, a decrease of the surface emissivity reduces the cooling of the surface but increases the cooling of the atmosphere above (Fig. 8). With the full 1D model, a decrease of the surface emissivity reduces the cooling of the surface which increases its temperature (Fig. 9). The temperature of the atmosphere above also increases, but less, as the decrease of emissivity increases the cooling of the atmosphere.

When the temperature profile is prescribed, we previously noticed that neglecting the spectral correlation at the surface leads to strongly overestimate the atmospheric cooling just above the reflective surface (Fig. 8). With the 1D model, neglecting the spectral correlation leads to underestimate by a factor of 0.5 to 0.7 the temperature increase in the boundary layer due to the emissivity decrease (Fig. 9). This underestimate is even more important if the turbulent vertical mixing is neglected (not shown). Neglecting the spectral correlation also slightly increases the diurnal cycle of the atmospheric temperature near the surface (not shown).

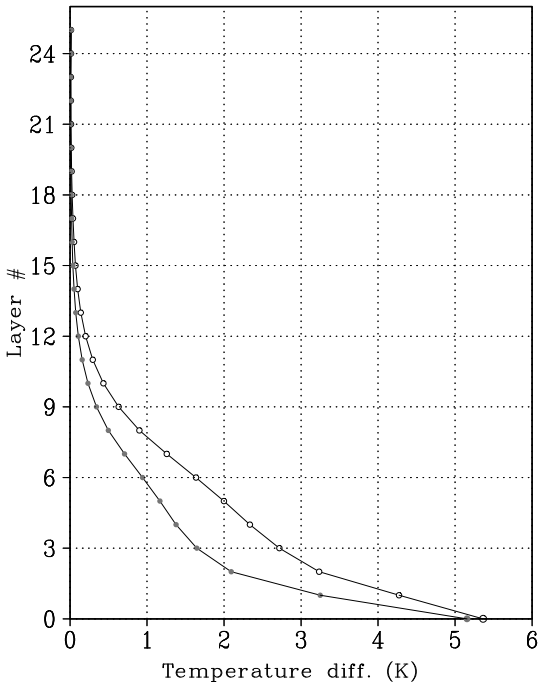

Figure 9: Vertical profile of the daily mean temperature difference due to a change in the surface reflectivity with an exact computation (open circle) and neglecting spectral correlation at the surface (closed circle). The temperatures of a run with a slightly reflective surface ($\epsilon_s = 0.9$) are compared to a run with a non reflective surface ($\epsilon_s = 1$). The runs are 10 days long, have the same initial state and are performed with the single column version of the Martian GCM. Diurnally averaged temperature differences are plotted for the last day. The vertical axis is the atmospheric layer number.

3.4 Computing vertical fluxes

In a general way there is no direct relationship between upward and downward fluxes and net exchanges. Only the net radiative fluxes may be directly expressed as a function of net exchanges. For instance, the net fluxes at the top of atmosphere $F^n_{N+\frac{1}{2}}$ reads:

$$F^n_{N+\frac{1}{2}} = \sum_{k=0}^{N} \psi_{N+1,k} \tag{33}$$

$$= \sum_{k=0}^{N} \sum_{m} \overline{\xi}^m_{N+1,k} \bar{B}^m_k \tag{34}$$

where N is the number of vertical layers, $k = 0$ stands for ground and $k = N + 1$ stands for space.

The optical exchange factors $\overline{\xi}$ present in Eq. 34 are comparable to the so-called weighting functions used to invert satellite radiative measurements. Therefore NEF should be a useful framework to assimilate those measurements in GCMs.

In the atmosphere, the net flux at level $i + \frac{1}{2}$ is equal to the net exchange between all the meshes below $i + \frac{1}{2}$ and all the meshes above $i + \frac{1}{2}$:

$$F^n_{i+\frac{1}{2}} = \sum_{j=i+1}^{N+1} \sum_{k=0}^{i} \psi_{j,k} \tag{35}$$

If one realy wants the values of the upward and downward fluxes, they may be approximated assuming each atmospheric layer is isothermal. If the optical exchange factors $\widetilde{\xi}$ have been computed with this assumption, the upward flux at level $i + \frac{1}{2}$ is equal to the flux emitted by all the meshes below $i + \frac{1}{2}$ and absorbed by all the meshes above $i + \frac{1}{2}$:

$$F^+_{i+\frac{1}{2}} = \sum_{j=0}^{i} \sum_{k=i+1}^{N+1} \widetilde{\xi}_{j,k} \bar{B}_j \tag{36}$$

Note that the errors on fluxes arising from the isothermal hypothesis are much smaller than the error on net exchanges between adjacent layers due to the same hypothesis. The same way, the downward flux at lever $i + \frac{1}{2}$ is equal to the flux emitted by all the meshes above $i + \frac{1}{2}$ and absorbed by all the meshes below $i + \frac{1}{2}$:

$$F^-_{i+\frac{1}{2}} = \sum_{j=0}^{i} \sum_{k=i+1}^{N+1} \widetilde{\xi}_{j,k} \bar{B}_k \tag{37}$$

4 Time integration

4.1 Numerical instabilities in the high atmosphere

When the atmospheric vertical resolution increases, numerical instabilities appear in the Martian GCM in the high atmosphere and they may increase dramatically. This problem has also been encountered in some GCM of the Earth atmosphere and specific stabilization techniques are commonly used to bypass this difficulty. Here we analyze the reasons of this difficulty and we propose a solution that takes advantage of the NEF.

In the original Martian model, the raditative transfer is integrated with an explicit time scheme, the evolution between times t and $t+\delta t$ of the temperature of layer i beeing computed from a computation of the heating rate $\psi_i^t = \sum_j \xi_{ij}^t (B_j^t - B_i^t)$ at time t as

$$T_i^{t+\delta t} = T_i^t + \frac{\psi_i^t \delta t}{m_i C_p} \tag{38}$$

In the upper atmosphere, the mass m_i of the atmospheric layers becomes very low, reducing they thermal capacitance. As a consequence, strong numerical oscillations appear for large time steps if the variations of ψ_i with temperature, within the time-step, are not taken into account.

A well-known solution to this problem consists in replacing ψ_i^t in Eq 38 by $\psi_i^{(\alpha)} = (1-\alpha)\psi_i^t + \alpha\psi_i^{t+\delta t}$. With those notations, the temporal scheme covers the cases of explicit ($\alpha = 0$), implicit ($\alpha = 1$) and semi-implicit ($\alpha = 1/2$) schemes. For $\alpha \neq 0$, the scheme is no more explicit and requires an inversion procedure. The net exchange formalism offers a simple practical solution to this problem. Based on the analysis above, it can be assumed that only the blackbody emissions B_i vary during the time-step while the optical coefficients do not. Also it can be assumed that only the exchanges with adjacent layers ($i \pm 1$) and boundaries (b) vary while the exchanges with distant layers are unmodified. With these approximations, and after linearization of the Planck function,

$$\psi_i^{(\alpha)} = \psi_i^t + \alpha \sum_{j=i\pm1,b} \xi_{ij}^t \left[\frac{dB}{dT}|_{T_j} (T_j^{t+\delta t} - T_j^t) - \frac{dB}{dT}|_{|T_i} (T_i^{t+\delta t} - T_i^t) \right] \tag{39}$$

If in addition we do not consider the variation of T_b within the time-step (which is exact for space and not a problem for the surface when computing the heating rates in the upper atmosphere), the temperature at time $t+\delta t$ is obtained from that at time t through the inversion of a tridiagonal matrix, for a low CPU cost.

This approach, implemented in the Martian GCM with $\alpha = 1/2$, is very efficient and supresses all the numerical oscillations in the upper atmosphere.

4.2 Saving computer time

The computation cost of the LW radiative code is known to be very important in most GCMs. Solutions have been proposed and implemented to reduce this computation time. Generally the full radiative code is computed only one out of N time steps, and approximations are used to interpolate the LW cooling rates between those N time steps. The simplest time interpolation scheme is to maintain constant the cooling rates during this period. This is the case in the original Martian GCM where the radiative code is computed one out of two time steps (each 1 hour).

On Mars, the surface temperature diurnal cycle is as high as $100K$ and the time interpolation method has to reproduce the effects of this diurnal cycle. The NEF provides an easy answer to this problem. Since the Planck function dominates the variations of the radiative exchanges, the Planck function will be computed at each time step while computing the optical factors $\overline{\xi}_{i,j}$ only one out of N time steps. A second level of optimisation consist in computing the optical exchange factors corresponding to the most important exchange rates (see Sec. 2.4) more frequently than the others. Once again, the NEF ensures that the above approximation will not alter the energy conservation and the reciprocity principle (Sec. 2.1). Practically all the optical exchange factors are scattered in three groups : the exchange factors between each atmospheric layer i and (1) its adjacent atmospheric layers, (2) the distant atmospheric layers (i.e. the other atmospheric layer) and (3) the boundaries (i.e. surface and space).

We present numerical tests performed using the single column version of our GCM. The runs last 50 days and the comparison between runs is performed using the results of the two last days. For these two days, we computed the atmospheric temperature difference between each run and the reference run. The mean and the RMS of this difference allows a quick comparison between them (Table 2). In the reference run (case # 1), the full LW code is called at each time step of the physics, i.e. every 30 Martian minutes). Case # 2 corresponds to what was implemented in the original version of our GCM: the full LW code is called one out of two time steps of the physic, i.e. every Martian hour, and the LW cooling rates are constant during this period. Computing all the optical exchange fac-

tors only once a day (case # 3) leads to an error only slightly greater than computing all the LW radiative code one out of two time steps (case # 2), but requires a much smaller CPU time. This result illustrates that the diurnal variations of the optical exchange factors are not very important compared to the diurnal variations of the Planck function.

As mentioned above, one may compute the most important exchange factors more frequency than the other. Computing the optical exchange factors with boundaries at each time step highly reduces the error while it only slightly increases the CPU time (case #4). Computing the exchange factors with adjacent layers at each time step slightly reduces the error while strongly increasing the CPU time (case #5).

Computing exchange factors only once a day may introduce a significant bias for long term simulations as the diurnal cycle is very badly sampled. We choose to compute all the exchange factors at least four times a day (case # 7-10). Computing the exchange factors with boundaries at each time step (30') and the other exchange factors every 6 hours (case # 8) produces much smaller errors than the original solution (case #2) while being two times less consuming. Another important advantage of this solution is that the number of exchange factors with boundaries increases linearly with the number N of vertical layers. The number of the other exchange factors are still proportional to N^2 but they are computed much less frequently and the required CPU time is therefore negligible: the CPU time will increase almost linearly with N and no more as a function of N^2 as for all the absorbtivity-emissivity methods.

If higher accuracy levels are required, a more frequent computation of the exchanges factors with both the boundaries and the adjacent layers is a good solution (case # 10). The errors are negligible and the CPU time is divided by a factor of two compared to the reference solution (case #1).

5 Summary and conclusion

In the present paper, a radiative code based on a flux formulation has been reformulated into a radiative code based on the NEF. This formulation has been proposed by Green (1967) but has not be often used since this time.

The graphical representation of the net exchange matrix appears to be a meaningful tool to analyze the radiative exchanges and the radiative budgets in the atmosphere. In the case of Mars, the exchange between a layer and space (the cooling to space) and the exchanges between a layer and its two adjacent layers are by far the dominant contributions to the radiative budgets. The exchange with space explains the general trend of the radiative budget with altitude. The exchanges with adjacent layers play a key role as they dump the temperature oscillations due to the various atmospheric waves.

A key point of the NEF is that it ensures both the energy conservation and the reciprocity principle whatever the errors or approximations are made when computing the optical exchange factors.

The net exchange between meshes is equal to the product of an optical exchange factors and the Planck function difference between the two meshes. This allows one to analyze separately the role of the optical properties of the atmosphere and the role of the temperature profile. The optical exchange factors are very expensive to compute and they vary slowly with time. On the contrary, the Planck function strongly depends on temperature, that strongly varies during a day, but is very fast to compute. Computing the optical exchange factors and the Planck function at different time steps is therefore of immediate interest. Moreover, because the NEF ensures both the energy conservation and the reciprocity principle, some of the exchange factors (the most important) may be computed more frequently than others. These possibilities give various opportunities to reduce the CPU time without loosing accuracy. Some possibilities have been explored in this paper. In particular we have shown that the most important terms are the exchanges with boundaries, number of which is proportional to the number N of vertical layers. Computing those terms more frequently than the others leads the CPU time to increase proportionally to N and not proportionally to N^2 as in all the absorbtivity/emissivity methods.

Another consequence of the splitting of the net exchange rates into optical exchange factors and Planck function differences is the possibility to linearize the Planck function for all or parts of the net exchanges. This allows us to implement implicit or semi-implicit algorithms at a low numerical cost (inversion of a tridiag-

case #	Computation periode of the net exchanges and the radiative budgets	the exchange factors with adjacent layers	boundaries	distant layers	Atm. temperature difference (K) mean	RMS	Normalized CPU time of the LW radiative code
1	30´	30´	30´	30´	0.00	0.00	1.00
2	1hr	1hr	1hr	1hr	-0.10	0.38	0.50
3	30´	1dy	1dy	1dy	0.32	0.38	0.15
4	30´	1dy	30´	1dy	-0.08	0.16	0.21
5	30´	30´	1dy	1dy	0.27	0.33	0.46
6	30´	30´	30´	1dy	-0.10	0.13	0.54
7	30´	6hr	6hr	6hr	0.21	0.20	0.16
8	30´	6hr	30´	6hr	0.01	0.05	0.25
9	30´	30´	6hr	6hr	0.18	0.20	0.47
10	30´	30´	30´	6hr	-0.01	0.02	0.52

Table 2: Comparison between the various time interpolation schemes.

onal matrix associated with exchanges between adjacent layers).

In our original radiative code (as well as in other codes), reflections at the surface are considered in a crude way: the reflected part of the downward radiation and the radiation emitted by the surface are supposed to have the same spectrum. We have shown that this approximation leads to highly overestimate the cooling of the atmosphere above the surface. The reason is that the spectrum of the downward radiation strongly depends on the gas absorption spectrum and is therefore very different from the spectrum of the radiation emitted by the surface. An exact computation is possible but double the CPU time.

A drawback of the NEF is that only the net flux in the atmosphere can be directly deduced from the net exchanges, not the upward and downward fluxes (although they are of experimental interests). Nevertheless we have shown that they can be estimated with a few more assumptions. On the other hand, the optical exchange factor between each gas layer and space does correspond to the so-called weighting function used to invert satellite flux measurements. Therefore a radiative code based on the NEF might be well suited for assimilation of satellite radiances.

The radiative code presented here is used in the last version of the LMD GCM of Mars (Forget et al., 1999). In addition to the absorption by gases presented in this paper, the effects of aerosols is also considered. Outside the two CO_2 wide bands, both absorption and scattering effect are computed using the algorithm of Toon et al. (1989). Inside the two CO_2 wide bands, only absorption by the aerosols is considered, scattering being neglected. This is consistent with previous studies that show that scattering by dust aerosols has the highest impact in window regions of the atmosphere (e.g. Dufresne et al., 2002). Currently a radiative code based on the NEF, that uses a ck-method for the spectral integration and that also considers scattering is under progress for the Venus planet.

6 Acknowledgments

This work was supported by the European Space Agency through ESTEC TRP contract 11369/95/NL/JG. The graphics have been made with the user friendly and public domain graphical package GrADS originally developed by Brian Dotty (COLA, support@grads.iges.org). We thanks the two anonymous reviewers for their very constructive comments.

References

Bresser, G., A. Manning, S. Pawson, and C. Rodgers, 1995, A new parameterization of scale-dependent radiative rates in the stratosphere, *J. Atmos. Sci.*, **52**, 4429–4447.

Cherkaoui, M., J.-L. Dufresne, R. Fournier, J.-Y. Grandpeix, and A. Lahellec, 1996, Monte-Carlo simulation of radiation in gases with a narrow-band model and a net-exchange formulation, *ASME J. of Heat Transfer*, **118**, 401–407.

Cherkaoui, M., J.-L. Dufresne, R. Fournier, J.-Y. Grandpeix, and A. Lahellec, 1998, Radiative net exchange formulation within one dimensional gas enclosures with reflective surfaces, *ASME J. of Heat Transfer*, **120**, 275–278.

Curtis, A., R., 1956, The computation of radiative heating rates in the atmosphere, *Proc. Roy. Soc.*, **A 236**, 148–156.

De Lataillade, A., J.-L. Dufresne, M. El Hafi, V. Eymet, and R. Fournier, 2002, A net exchange Monte Carlo approach to radiation in optically thick systems, *J. Quant. Spectrosc. Radiat. Transfer*, **75**, 529–538.

Dufresne, J.-L., R. Fournier, and J.-Y. Grandpeix, 1998, The Monte-Carlo exchange method for radiative budget computation in a gas-filled two dimensional enclosure, *Comptes Rendus de l'Académie des Sciences, Série II b*, **326**, 33–38.

Dufresne, J.-L., R. Fournier, and J.-Y. Grandpeix, 1999, Inverse gaussian k-distributions, *J. Quant. Spectrosc. Radiat. Transfer*, **61**, 433–441.

Dufresne, J.-L., C. Gautier, P. Ricchiazzi, and Y. Fouquart, 2002, Longwave scattering effects of mineral aerosols, *J. Atmos. Sci.*, **59**, 1959–1966.

Elsasser, W. M., 1942, *Heat Transfer by Infrared Radiation in the Atmosphere*, vol. 6 of *Harvard Meteorol. Stud.*, Harvard University Press.

Eymet, V., J.-L. Dufresne, P. Ricchiazzi, R. Fournier, and S. Blanco, 2004, Longwave radiative analysis of cloudy scattering atmospheres using a net exchange formulation, *Atmospheric Research*, **72**, 239–261.

Fels, S., and M. Schwarzkopf, 1975, The simplified exchange approximation: A new method for radiative transfer calculations, *J. Atmos. Sci.*, **32**, 1475–1488.

Forget, F., J. B. Pollack, and G. B. Hansen, 1995, Low brightness temperatures of Martian polar caps: CO_2 clouds or low surface emissivity?, *J. Geophys. Res.*, **100**, 21,119–21,234.

Forget, F., F. Hourdin, and O. Talagrand, 1998, CO_2 snow fall on Mars: Simulation with a general circulation model, *Icarus*, **131**, 302–316.

Forget, F., F. Hourdin, R. Fournier, C. Hourdin, O. Talagrand, M. Collins, S. R. Lewis, P. L. Read, and J.-P. Huot., 1999, Improved general circulation models of the Martian atmosphere from the surface to above 80 km, *J. Geophys. Res.*, **104**, 24,155–24,176.

Goody, R. M., and Y. L. Yung, 1989, *Atmospheric Radiation, Theoretical Basis*, Oxford University Press., second edition, 519 pp.

Green, J. S. A., 1967, Division of radiative streams into internal transfer and cooling to space, *Quarterly J. of the Royal Meteorological Society*, **93**, 371–372.

Hottel, H. C., and A. F. Sarofim, 1967, *Radiative Transfer*, McGraw-Hill, 520 pp.

Hourdin, F., P. Le Van, F. Forget, and O. Talagrand, 1993, Meteorological variability and the annual surface pressure cycle on Mars, *J. Atmos. Sci.*, **50**, 3625–3640.

Hourdin, F., 1992, A new representation of the CO_2 15 μm band for a Martian general circulation model, *J. Geophys. Res.*, **97**, 18,319–18,335.

Joseph, J. M., and R. Bursztyn, 1976, A radiative cooling model in the thermal infrared for application to models of the general circulation, *J. of Applied Meteorology*, **15**, 319–325.

Leovy, C., and Y. Mintz, 1969, Numerical simulation of the atmospheric circulation and climate of Mars, *J. Atmos. Sci.*, **26**, 1167–1190.

Lewis, S. R., M. Collins, P. L. Read, F. Forget, F. Hourdin, R. Fournier, C. Hourdin, O. Talagrand, and J.-P. Huot., 1999, A climate database for Mars, *J. Geophys. Res.*, **104**, 24,177–24,194.

Modest, M., 1992, The Monte Carlo method applied to gases with spectral line structure, *Numerical Heat Transfer, Part B*, **22**, 273–284.

Morcrette, J. J., L. Smith, and Y. Fouquart, 1986, Pressure and temperature dependence of the absorption in longwave radiation parametrizations, *Contrib. Atmos. Phys.*, **59**, 455–469.

Morcrette, J.-J., 1990, Impact of changes to the radiation transfer parameterizations plus cloud optical properties in the ECMWF model, *Mon. Wea. Rev.*, **118**, 847–873.

Pollack, J. B., C. B. Leovy, P. W. Greiman, and Y. Mintz, 1981, A Martian General Circulation Model experiment with large topography, *J. Atmos. Sci.*, **38**, 3–29.

Ritter, B., and J.-F. Geleyn, 1992, A comprehensive radiation scheme for numerical weather prediction models with potential applications in climate simulations, *Mon. Wea. Rev.*, **120**, 303–25.

Rodgers, C. D., and C. D. Walshaw, 1966, The computation of infra-red cooling rate in planetary atmospheres, *Q. J. R. Meteorol. Soc.*, **92**, 67–92.

Santee, M., and D. Crisp, 1993, Thermal structure and dust loading of the Martian atmosphere during late southern summer: Mariner 9 revisited, *J. Geophys. Res.*, **98**, 3261–3279.

Schwarzkopf, D., and S. Fels, 1991, The simplified exchange method revisited: an accurate, rapid method for computation of infrared cooling rates and fluxes, *J. Geophys. Res.*, **96**, 9075–9096.

Seiff, A., 1982, Post-Viking models for the stucture of the summer atmosphere of Mars, *Adv. Space Res.*, **2**, 3–17.

Toon, O. B., C. P. McKay, T. P. Ackerman, and K. Santhanam, 1989, Rapid calculation of radiative heating rates and photodissociation rates in inhomogeneous multiple scattering atmospheres, *J. Geophys. Res.*, **94**, 16,287–16,301.

Zhang, L., A. Soufiani, and J. Taine, 1988, Spectral correlated and non-correlated radiative transfer in a finite axisymmetric system containing an absorbing and emitting real gas-particle mixture, *International J. of Heat and Mass Transfer*, **31**, 2261–2272.

7 Appendix

7.1 Sub-grid temperature quadratic profile

We consider here an atmosphere with a temperature profile that is compatible with a second order blackbody intensity profile within the considered spectral band

$$B(z) = az^2 + bz + c. \tag{40}$$

We also assume that absorption coefficients are uniform. Under these assumptions, the net exchanges between two layers i and j (Eq. 12) of thickness e separated by a layer of thickness l lead to the following double integral:

$$\psi_{i,j} = \int_{\Delta\nu} d\nu \int_{-l/2-e}^{-l/2} dx \int_{+l/2}^{+l/2+e} dy\ k_\nu^2 \exp[-k_\nu(y-x)][B(y)-B(x)] \tag{41}$$

$$= \int_{\Delta\nu} d\nu \int_0^e dx \int_0^e dy\ k_\nu^2 \exp[-k_\nu(x+y)] \exp(-k_\nu l)[B(y+l/2)-B(-x-l/2)] \tag{42}$$

$$= b \int_{\Delta\nu} d\nu \exp\left(-k_\nu l\right)\left[1-\exp\left(-k_\nu e\right)\right]\left\{\left(l+2/k_\nu\right)\left[1-\exp\left(-k_\nu e\right)\right]-2e\exp\left(-k_\nu e\right)\right\} \tag{43}$$

This is obtained by expanding the expression of B in Eq. 41. The terms with c directly disapear. The double integral of the terms with a is equal to zero. Only the terms with b remain.

Under the same assumptions, Eq. 40 leads to

$$b = \frac{\overline{B}_j - \overline{B}_i}{l+e} \tag{44}$$

with $\overline{B}_i$ and $\overline{B}_j$ the average blackbody intensities of layers i and j.

Therefore, Eq. 43 depends only on the layer average of B, which means that all quadratic profile that meet the layer averages have the same first order terms and therefore lead to identical net exchange rates. In particular, the linear subgrid profile approximation used in Sec. 3.2 for adjacent layer net exchange computations is therefore equivalent to a second order approximation.

Note that this demonstration is only valid for conditions in which layer thicknesses are comparable and that the reasoning is made with blackbody intensity layer averages, whereas GCM outputs are temperature averages. Practical use therefore requires that blackbody intensities may be confidently linearized as fonction of temperature, which implies limited temperatures gradients.

7.2 Errors due to the isothermal layer approximation

The same analysis may also be used to justify the use of the isothermal layer assumption for non adjacent layer net exchange computations. We consider an atmosphere with the same previous temperature profile that is compatible with a second order blackbody intensity profile within the considered spectral band. Under this assumption, the net exchange between two layers i and j (Eq. 12) of thickness e separated by a layer of thickness l may be approximated as

$$\tilde{\psi_{i,j}} = \int_{\Delta\nu} d\nu \exp(-k_\nu l)\left[1-\exp(-k_\nu e)\right]^2 \left(\overline{B}_j - \overline{B}_i\right) \tag{45}$$

$$= \int_{\Delta\nu} d\nu \exp(-k_\nu l)\left[1-\exp(-k_\nu e)\right]^2 b(l+e) \tag{46}$$

Using the exact expression of $\psi_{i,j}$ (Eq. 43), the corresponding relative error $\mathcal{E} = \frac{\psi-\tilde{\psi}}{\psi}$ in the optically thick limit writes:

$$\text{if } k_\nu e \gg 1 \text{ then } \mathcal{E} \approx \frac{2-k_\nu e}{2-k_\nu l}. \tag{47}$$

If the optical thickness between the two layers distant of l is also high ($k_\nu l \gg 1$), the relative error on the net exchange is $\mathcal{E} \approx \frac{e}{l}$, which means that the relative error on the net exchange between two layers due to the isothermal layer approximation decreases when the distance between the two layer increases.

One can be more precise when considering three contiguous layers, numbered 1, 2 and 3, of thickness e. We estimate the error made when computing the net exchanges between layer 1 and the two other layers, $\psi = \psi_{1,2} + \psi_{1,3}$, accounting for the exact sublayer profile for $\psi_{1,2}$ (i.e. for the adjacent layer) and using the isothermal layer assumption for $\psi_{1,3}$ (i.e. for the distant layer). With the same notation as here above with $l = e$, the corresponding relative error becomes:

$$\mathcal{E}_\nu = \frac{(k_\nu e - 2)[1 - \exp(-k_\nu e)] + 2k_\nu e \exp(-k_\nu e)}{(k_\nu e + 2)[1 - \exp(-k_\nu e)] - 2k_\nu e \exp(-k_\nu e) + \frac{1 - ae/b}{\exp(-k_\nu e)} \{2[1 - \exp(-k_\nu e)] - 2k_\nu e \exp(-k_\nu e)\}}$$

This relative error is 0 for small values of the optical thickness $k_\nu e$, reaches 5% for an optical thickness of 2, then decreases toward 0 when the optical thickness increases.